Anisotropic Colloidal Templating of 3D Ceramic, Semiconducting, Metallic, and Polymeric Architectures

Ming Fu, Kundan Chaudhary, Jonathan G. Lange, Ha Seong Kim, Jamie J. Juarez, Jennifer A. Lewis, and Paul V. Braun**

Three-dimensional (3D) mesostructured materials have attracted considerable attention due to their potential applications in photonics,[1,2] energy harvesting and storage,[3] sensors,[4] and catalysis.[5] These materials have been formed by methods including interference lithography,[6] multilayer microfabrication,[7] soft-template assisted synthesis,[8] direct writing,[9] interference lithography[10] and biological template replication,[11] as well as a diversified array of self-organization techniques.[1,12,13] Templating methods, especially those based on colloidal crystals,[13] are of particular interest due to their ease, low cost, and ability to form highly periodic structures with characteristic dimensions ranging from 10s of nm to several micrometers. Importantly, these methods enable decoupling of final templated material's chemistry from the initial mesoscale structure, significantly broadening the available set of materials over those which can be formed into templates. Current 3D colloidal structures are generally assembled from spherical, or in a few cases near-spherical (aspect ratio of 1.3 to 1.6)[14] building blocks, and hence function only as isotropic or nearly isotropic templates. To date, highly anisotropic templates have primarily been confined to two-dimensional (2D) architectures, such as anodically derived porous alumina[15] and silicon,[16] which yield templated materials with limited and poorly controlled connectivity in the lateral direction. The ability to create 3D anisotropic architectures over large areas with precisely patterned sub-micrometer features is therefore lacking. Here, we create horizontally and vertically aligned 3D templates assembled from anisotropic colloidal rods and demonstrate their transformation to unique inverse 3D ceramic, semiconducting, metallic and polymeric architectures with intertwining solid and porous features (**Scheme 1**).

We first created anisotropic building blocks composed of colloidal silica rods using a modified one-pot method recently reported by Kuijk and co-workers.[17,18] In the initial growth step, silica rods with a length (L) of 1.90 ± 0.20 μm and diameter (D) of 0.31 ± 0.05 μm are created. These rods are used as seeds in subsequent growth steps[19] to produce silica rods (L/D = 3.75) with final dimensions of L = 2.1 ± 0.2 μm and D = 0.56 ± 0.11 μm. The method is general and can be used to produce colloidal rods of varying size and aspect ratios with potential for electric field alignment.[14,18,20]

To produce horizontally and vertically aligned colloidal rod templates, we identified the optimal AC electric field strength and frequency for each desired configuration. Colloidal suspensions composed of 4–12 wt% rods with an aspect ratio, L/D = 3.75, are placed within the gap between the two ITO electrodes. Upon application of an AC electric field, the rods experience a torque, $\mathbf{T} = \mathbf{p} \times \mathbf{E}$, where dipole moment, $\mathbf{p} \sim L^3\mathbf{E}/\ln(4L/D)$, and $\mathbf{E}$ is the electric field strength.[21] To induce horizontal rod alignment, the optimal AC electric field strength and frequency ranged from 20–50 V/mm at 1–10 MHz. Under these conditions, the rods rapidly assemble into linear chains that are oriented along the direction of the applied field (**Figure 1**). To induce vertical rod alignment that persists during template drying, the optimal electric field strength ranged from 50–100 V/mm at a frequency of 25 kHz. At this lower frequency, electro-osmotic flow generated by counterion motion within the electric double layer surrounding each rod assists their assembly into dense, hexagonally close-packed (HCP) domains.[22] We quantified the number of rods coordinated (in plane) by six nearest neighbors using image analysis under each experimental condition studied, and report the degree of HCP alignment in Figure 1.[23] A high degree of HCP alignment is required to create stable templates, in which the vertical orientation of the rods are retained during drying.

We used these anisotropically aligned templates to create mesostructured hafnia (HfO_2), silicon (Si), nickel (Ni), and poly(methyl methacrylate) (PMMA), as outlined in Scheme 1. The rods are first dispersed in an aqueous solution at a concentration required to achieve the desired film thickness. A transverse or longitudinal AC electric field is applied with respect to the substrate (i.e., ITO or gold-coated substrates) depending on the desired orientation (Scheme 1b). The rods assemble with their long-axis parallel to the direction of applied electric field. As water evaporates, 3D rod templates with horizontal (Scheme 1c) or vertical orientation (Scheme 1d) are consolidated on the substrate. These templates are then used to create inverse structures of the desired material of interest (Scheme 1e). Specifically, HfO_2 is grown by atomic layer deposition (ALD), Si by static chemical vapor deposition (CVD), Ni by electrodeposition, and PMMA by in-situ polymerization.

Dr. M. Fu, J. G. Lange, H. S. Kim, Prof. P. V. Braun
Department of Materials Science and Engineering
Materials Research Laboratory
and Beckman Institute
University of Illinois at Urbana-Champaign
Urbana, Illinois, 61801, USA
E-mail: pbraun@illinois.edu
K. Chaudhary, Dr. J. J. Juarez, Prof. J. A. Lewis
School of Engineering and Applied Sciences and
Wyss Institute for Biologically Inspired Engineering
Harvard University
Cambridge, MA, 02138, USA
E-mail: jalewis@seas.harvard.edu

DOI: 10.1002/adma.201304809

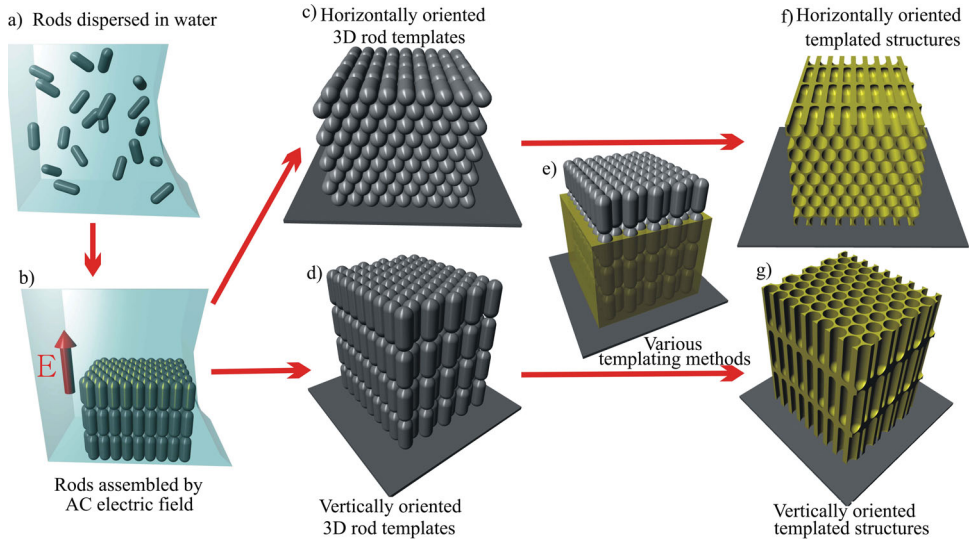

Scheme 1. Schematic illustrations of the rod assembly process along with templating approaches and the resultant architectures. (a) Silica nanorods dispersed in water. (b) Rods assembled using a combined electric field and self-assembly process both parallel (c) and normal (d) to the substrate. (e) Illustration of bottom-up (non-conformal) infilling. (f, g) Resulting horizontally and vertically oriented 3D rod templated structures.

Finally, the silica rods are removed from these structures by etching them using an HF solution. Each functional material is templated as both horizontally and vertically oriented inverse mesoporous architectures.

Figure 2a–d presents SEM images of 3D rod templates with the silica rods aligned horizontally with respect to the substrate. In Figure 2a, **3**D rod assembly is controlled solely by applying a horizontal AC electric field without optimizing the drying conditions. The major axis of colloidal silica rods aligns parallel to the direction of electric field. However, several rods are not well aligned. Using an optimized angular or micro-capillary drying method alone, the rods can be self-assembled into well-organized morphologies (Figure 2b). The long axis of the rods is always parallel to the substrate, however, the rod direction is still not uniform. Adjacent rods tend to close-pack, however, domains with different orientations persist. Combining the AC electric field with this optimized drying method yields a highly regular array of rods (Figure 2c). The thickness of the horizontally aligned structures can be controlled from tens to hundreds of layers depending on the initial rod concentration in suspension. A typical cross-section of the horizontally oriented rods is shown in Figure 2d, in which all rods are parallel to the substrate with their long-axis perpendicular to the cross-section view. As expected, the rods tend to assemble into a hexagonal close-packed arrangement perpendicular to their long-axis (inset of Figure 2d).

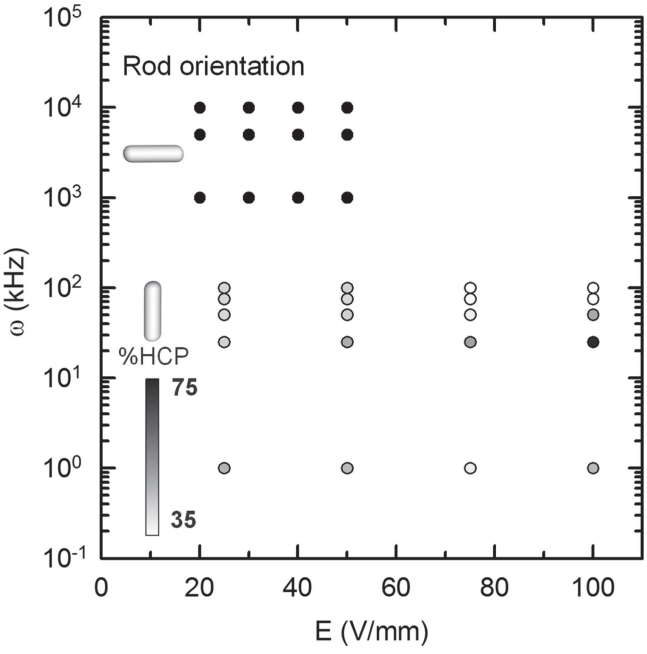

Figure 1. Phase diagram depicting horizontal (black circles) and vertical (grayscale circles) rod alignment as a function of applied frequency and electric field. [Note: The optimal conditions for vertical rod alignment occurred at 100 V/mm at 25 kHz (darkest gray circle)].

Using these horizontally aligned rods as templates, HfO_2, Si, Ni, and PMMA-based inverse structures can be formed (Figure 2e–i). Starting with HfO_2 (Figure 2e,f), which is grown via the conformal ALD process, the cylindrical shells formed by removal of the rods are aligned uniformly in same direction parallel to the surface. In the FIB-SEM image (Figure 2f), both the top (surface) and hexagonal cross-sections can be observed. The HfO_2 coating is intentionally thick, resulting in a near replica of the void space provided by the silica rods (complete filling is not possible due to 'pinch-off'[24]). Top-views of Si, Ni, and PMMA (for PMMA, imaging is from the substrate side after substrate removal) structures templated by horizontally aligned rod templates are shown in Figure 2g-i. Due to the nearest neighbor configuration within these colloidal rod templates, there are line contacts between each embedded pore. The similarity of the HfO_2 and Si structures is expected, as they

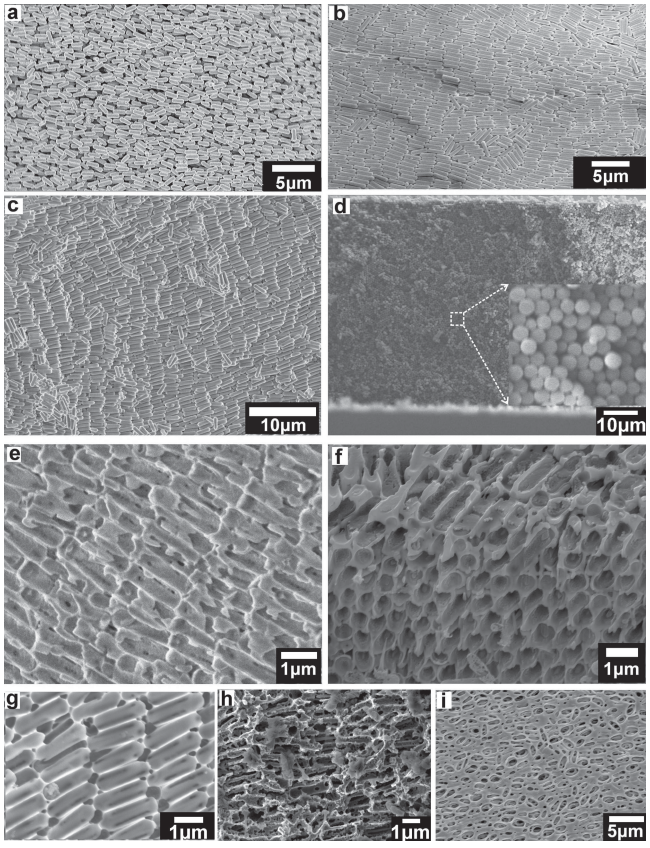

Figure 2. SEM images of horizontally aligned colloidal rods and templated mesoscale architectures. Top-views of (a) horizontally aligned colloidal silica rods via electric-field assisted assembly, (b) horizontally aligned silica rods via self-assembly by angular drying method, (c) horizontally aligned silica rods by combined surface-tension-driven self-assembly and electric-field assisted assembly. (d) Cross-sectional image of silica rods with horizontal alignment. (e) Top- and (f) cross-sectional views of rod templated HfO_2 structures. Top-view SEM images of rod templated (g) Si, (h) Ni, and (i) PMMA structures.

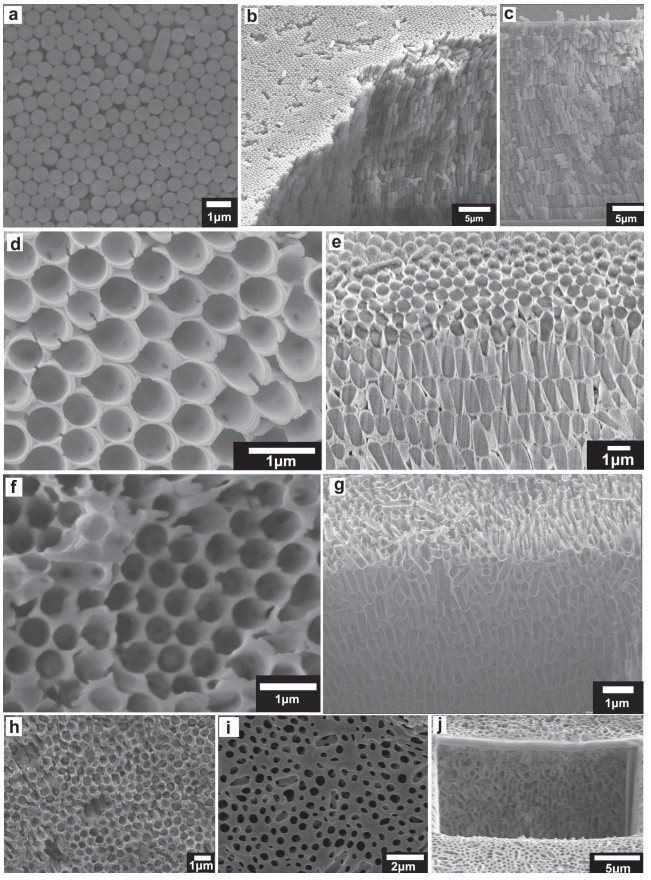

Figure 3. Vertically aligned colloidal rod templates and inverse mesoscale architectures. (a-c) SEM images of vertically aligned silica rods: (a) top, (b) angled, and (c) cross-sectional views. (d) Top and (e) cross-sectional SEM images of vertically aligned rod templated HfO_2 structures. (f) Top and (g) cross-sectional SEM images of vertically aligned rod templated Si structures. (h) Top-view SEM image of vertically aligned rod templated Ni. (i) Top and (j) cross-sectional SEM images of vertically aligned rod templated PMMA structures.

are both grown conformally on the silica rods from the vapor phase. SEM images of the HfO_2 and Si are acquired after ion-beam etching of the thin layer present at the top of each 3D structure after materials deposition. Removal of the overlayer is required to enable the etchant to access the rods within the interior of the structure. Ni electrodeposition initiates at the substrate and surface etching is not required since the electrodeposition is terminated before the Ni overgrows the template. The templated PMMA structures tend to produce ellipsoidal pores because of deformation of PMMA, due to volumetric shrinkage during either polymerization or silica etching. However, even the PMMA structures present a generally uniform mesoscale architecture.

Figure 3a presents a top view of the vertically oriented, colloidal rod templates. Their surface possesses a 2D hexagonal close-packed geometry; only a few rods are observed to be lying down horizontally on the top surface of the structure. Figure 3b is an angular view SEM image of the vertically assembled rods revealing both the ordered arrangement of rods on the surface plane (left-top in Figure 3b) and their uniform vertical orientation along their long-axis (right-bottom side in Figure 3b). In the cross-sectional view (Figure 3c), one finds that nearly all the rods exhibit uniform vertical alignment and are approximately close-packed. Similar to the case for the horizontally oriented rods, these vertically oriented templates are also suitable for growth of a diverse array of functional materials. Figure 3d shows a typical top-view SEM image of a HfO_2 rod inverse structure, which consists of hexagonal close-packed, vertically aligned hollow cylinders. The vertically aligned pores are also evident in the FIB-SEM image (Figure 3e). In Figure 3e, the silica rods have not been removed, enabling easier visualization of the pores that remain in the structure due to pinch-off.[24] Figure 3f and 3g show typical top and side-view SEM images, respectively, of a Si rod inverse structure. Note, in Figure 3g, the rods have been removed. Top view of the vertically aligned, rod templated Ni (Figure 3h), and top and cross-sectional views of rod templated PMMA are shown in Figures 3h–j. There are some differences between the templated Ni (Figure 3h) and HfO_2 (Figure 3d) structures. Because Ni infills from the bottom up, there are no voids at

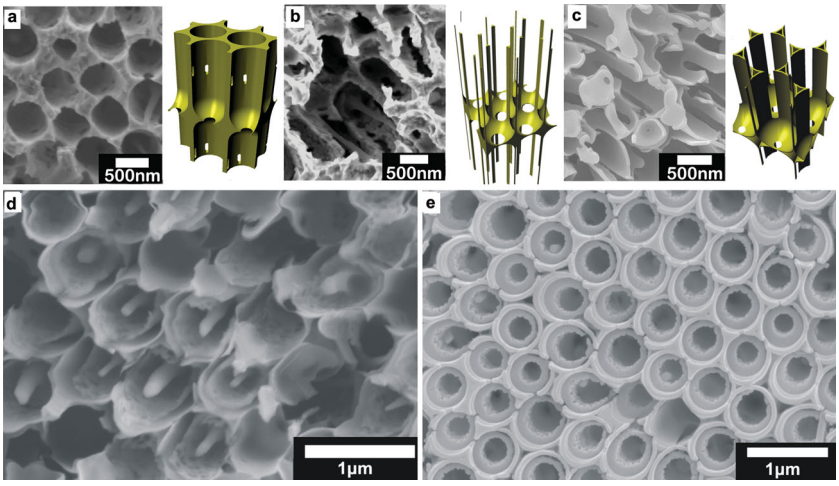

Figure 4. Morphologies induced by different infilling and etching techniques. (a-c) SEM images (left), and schematics (right) after template removal. Template was (a) fully filled with Ni, (b) partially filled with Ni, and (c) conformally coated with HfO_2. (d,e) Top-view SEM images of inverse (d) HfO_2 and (e) Si structures fabricated using vertically aligned rod templates, where the silica rods are not fully etched.

the interstitial spaces between the rods, while for the conformally deposited HfO_2, due to pinch-off during HfO_2 deposition, small voids appear. The Ni structures are not as smooth as the HfO_2 structures, perhaps because Ni may be etched slightly by the nickel electrodeposition solution. The PMMA completely fills the structure as expected, and the surface mainly consists of (slightly distorted) round holes. Only a few voids, induced by rods lying horizontally, are present on the surface.

These 3D colloidal rod templates yield anisotropic morphologies that are not possible to achieve using either spherical colloidal crystal or 2D anisotropic templates. In particular, the connectivity parallel and perpendicular to the rods is quite different. For touching rods, at the end of each rod-like void, only small spherical interconnect windows appear, while perpendicular to the voids, a long vertical slot-like pore is formed. While this is most apparent in Figure 3d, it is present in all the systems. The SEM images and schematics in **Figure 4**a,b provide nice examples of complete and partial infilling of Ni. When the coating is not very thick, the vertical channels formed on the wall between two of the templated rod-like voids are more obvious. In some regions of the electrodeposited structure, probably because of non-uniform current densities in our electrodeposition cell, the Ni does not fully fill the template, and large interconnect windows and only thin ligaments are formed parallel to the rods (Figure 4b). Figure 4c shows a typical thin HfO_2 structure that contains many vertical channels. As expected, we observe in the SEM images that the effect of pinch-off is the same for the vertically and horizontally aligned channels (e.g., Figures 2f, 3d,e and S1) since the minimum pore dimensions, which lead to pinch-off, are the same regardless of the rod orientation.

During the silica rod etching process, several interesting hybrid morphologies can be formed due to the differential etch rates between the initial (seed) cores and subsequently grown outer layers of the synthesized silica rods. Figures 4d and S2 show SEM images of horizontally and vertically oriented Si rod templated structures when the silica rods are incompletely removed by the HF-ethanol solution. During the etching process, the rod cores and shells are not removed at the same rates. Figure 4e shows another typical SEM image of templated structures in which the silica rods are incompletely removed in HF-water solution. In contrast to HF-ethanol, when etched in HF-water, the cores of the silica rods are removed before their shells, leaving hollow silica cylinders around each of the pore within the templated HfO_2 architecture.

We note that randomly oriented, colloidal rods can also serve to template 3D structures, and these structures are far easier to assemble then well aligned rods. Figure S3 shows a typical Ni structure templated using randomly oriented rods. Their void fraction is much higher than well-aligned, densely packed colloidal rod templates; hence, the volume fraction of the infilled material is considerably higher. However, the connectivity between pore channels in these structures is poorly controlled relative to those produced by aligned templates.

In conclusion, we have successfully demonstrated a general technique for fabricating 3D anisotropic mesoscale architectures using colloidal rod templates. The templates can be horizontally or vertically aligned, with a high degree of uniformity, relative to the substrate via a combined process of electric-field assisted and self-assembly. The inverse 3D anisotropic structures are formed from all the major classes of materials: ceramics, semiconductors, metals, and polymers using both bottom-up and conformal template infilling strategies. These 3D mesoscale architectures hold significant promise for applications in which anisotropic transport, electrical, or optical properties are important, including electrochemical energy storage, thermal management, sensors, and photonics.

Experimental Section

Anisotropic Rod Synthesis: Silica rods are synthesized using one-pot synthesis technique developed by Kuijk and co-workers.[18] Briefly, 300 ml of pentanol and 30 g of polyvinylpyrrolidone (PVP) are added to a 500 ml round bottom flask and sonicated for 3–4 h until the PVP is fully dissolved. Next, 30 ml ethanol followed by 8.4 ml of DI water is added to the flask. Then, 2 ml of 0.18 M sodium citrate dihydrate (5.3 g in 100 ml DI water) is added and the flask is shaken 15–20 times by hand. The mixing results in formation of an emulsion.

We modified the original procedure reported by Kuijk and co-workers to include a filtration step to generate nearly monodisperse emulsion droplets. Using a syringe pump (flow rate of 50 ml/h) a 0.1 μm pore size filter is used to filter the emulsion droplets and the filtrate is collected in a clean round bottom flask. 6.75 ml of ammonium hydroxide is added and the flask is shaken by hand 15–20 times before adding 3 ml tetraethylorthosilicate (TEOS). The flask is again shaken by hand 10 times and left undisturbed at 20 °C for 17 h.

When the reaction is complete, the silica rod suspension is centrifuged in ethanol at 3000 rpm for 1 h and the supernatant is removed. This step is repeated twice more at 1500 rpm for 15 min. After the ethanol wash, the rod suspension is centrifuged in DI water at 1500 for 15 min until the pH of the supernatant is neutral. To improve

the size uniformity, the rods are further centrifuged 5 times in ethanol at a lower centrifugation speed of 1200 rpm for 10 min. This yields silica rods with a length (L) of 1.9 ± 0.2 µm and diameter (D) of 0.31 ± 0.05 µm. These seed particles are then grown using a seeded Stöber process. Monodisperse silica rods are added to a 50 ml ethanol in a 500 ml round bottom flask. The rod suspension is stirred using magnetic stir bar. Next, 6 ml ammonium hydroxide, 5 ml DI water, 0.5 ml TEOS are added in succession. After 6 h, 0.12 ml DI water and 0.5 ml TEOS are added every 3 h. 7 additions are performed to obtain ~0.5 g of rods (36% yield) with final dimensions of $L = 2.1 \pm 0.2$ µm and $D = 0.56 \pm 0.11$ µm. The rods are densified at 700 °C for 12 h after drying and then redispersed in water at the desired concentration.

Horizontal Rod Assembly: In the first method, two ~1 cm^2 gold electrode pads separated by a 200 µm gap are printed on a silicon or glass substrate. One drop of an aqueous 2–5% w/w silica rod suspension is placed on the substrate, and then covered with a hydrophobic glass slide yielding a ~300 µm gap between the top and bottom substrates. The edges of the resulting cell are taped with scotch tape, a 20–50 V/mm, 1–10 MHz AC electric field is applied, and the water is allowed to slowly evaporate through gaps in the scotch tape. This guided assembly process is carried out at room temperature, where drying times in excess of 6 h are required. Using this method, the horizontally aligned rods between the two conducting pads are above an insulating region of the substrate, where Ni cannot be electrodeposited. Hence, for templating Ni, we carried out horizontal rod alignment on a conducting substrate. In this second method, a hydrophobic glass slide is placed 75 µm above the ITO-coated substrate. The space between the substrates is partially filled with an aqueous 10% w/w silica rod suspension, such that the resulting flattened droplet of rod suspension only contacted one edge of the sandwich. The droplet remained pinned to this edge as water evaporation ensues resulting in a horizontally aligned rod template on ITO coated glass suitable for Ni electrodeposition. Both these methods are generally termed the 'micro-capillary method'. Horizontally aligned rods could also be assembled by placing one drop of an aqueous 10% w/w silica rod suspension on a substrate lying at about 20° to the horizontal followed by drying at 45 °C (angular drying method).

Vertical Rod Assembly: Two parallel electrodes (ITO-coated glass or gold-coated Si) separated by a 75 µm gap are used for creating vertically aligned colloidal rod templates. When ITO electrodes are used, one electrode is immersed in a 0.5 wt% trichloro(perfluorooctyl)silane ethanol solution to render it hydrophobic prior to electrode assembly to assist the formation of discrete water columns between the top and bottom electrodes during solvent evaporation. A 5 µl drop of an aqueous 4–12% w/w silica rod suspension is placed on one of the electrodes, and sandwiched with a second electrode, forming an ~5 mm disk of the suspension. A 50–100 V/mm, 25 kHz AC electric field is then applied, while water is allowed to slowly evaporate over a period of at least 6 h.

Order Parameter: The tracked centers of vertically oriented rods are used to calculate an order parameter, $\langle C_6 \rangle$, defined as the average number of crystalline nearest neighbors in an ensemble.[25] The number of coordinated neighbors, N_C^i, to particle i are all particles j within a coordination radius, r_C, oriented at angles θ_{ij}. Identification of crystalline near neighbors is based on a six-fold bond orientational order parameter for particle i, ψ_6^i, given by,[26]

$$\psi_6^i = \frac{1}{N_C^i} \sum_{j=1}^{N_C^i} \left[e^{6\theta_{ij}\sqrt{-1}} \, r_{ij} \leq r_C \right] \tag{1}$$

which is used to determine crystalline connectivity, χ_6^{ij}, between particle i and a neighboring particle j as,[27]

$$\chi_6^{ij} = \frac{\left| \mathrm{Re}\left[\psi_6^i \psi_6^{j*} \right] \right|}{\left| \psi_6^i \psi_6^{j*} \right|} \tag{2}$$

where ψ_6^{i*} is the complex conjugate of ψ_6^i. The number of crystalline near neighbors, C_6^i, for particle i is,[23]

$$C_6^i = \sum_{j=1}^{N_C^i} \left[\begin{vmatrix} 1 & \chi_6^{ij} \geq 0.32 \\ 0 & \chi_6^{ij} < 0.32 \end{vmatrix} \right] \tag{3}$$

which is based on a criterion that a connection between particles i and j only be considered crystalline for $\chi_6^{ij} > 0.32$.[27] The value of $\langle C_6 \rangle$ is the average over all particles in an ensemble as,

$$\langle C_6 \rangle = \frac{1}{N} \sum_{i=1}^{N} C_6^i \tag{4}$$

The variable $\langle C_6 \rangle$ is averaged for every captured frame.

Anisotropic Template Infilling: HfO_2 is grown within horizontally and vertically oriented rod templates using 200–800 ALD cycles. In each ALD cycle (Savannah 100, Cambridge NanoTech), water and tetrakis(dimethylamido)hafnium(IV) exposure times are 0.015 s and 0.20 s, respectively, each followed by a 10 s pump time. The chamber is kept at 200 °C during the deposition process. Each ALD cycle conformally deposits ~0.8 Å HfO_2 on the individual rods throughout the oriented templates. Si is deposited from disilane using a static CVD system. The system is first evacuated to 10^{-6} mBar, then the chamber is charged with 520 mBar disilane and sealed. The sample chamber is heated to 350 °C and held for 3 h. A three-electrode system (Biologic VMP3) is used for Ni electrochemical deposition. The rod-coated on ITO or gold substrates are used as the working electrode, while a saturated calomel electrode (SCE) and a platinum foil served as a reference electrode and counter electrodes, respectively. A commercial nickel electrodeposition solution (nickel sulfamate, Technic Inc., #030179) is used. Ni is deposited via potentiostatic deposition at –0.9 V versus SCE for 2–6 h at room temperature. PMMA is polymerized in horizontal and vertical rod templates by fully filling the template with a 0.5 wt% azodiisobutyronitrile methyl methacrylate solution in a sealed glass vessel followed by heating to 55–70 °C for 30 h.

After Ni, HfO_2, Si, or PMMA is infilled, the silica rods are removed by immersing the 3D structure in various HF solutions. The inverse Ni architectures are immersed in a 7.2% HF, 7.8% water, 85% ethanol solution for 30 min. A 7.2% HF(aq) water solution or the same HF-ethanol solution is used to etch the HfO_2 and Si structures after removing an approximately 300–1000 nm thick surface layer by ion beam milling. The etching time varied from 10–30 min to partly or fully remove the silica rods. The PMMA structures are immersed in a 48% HF water solution (HF is extremely toxic and should be handled with appropriate personal protection and inside a fume hood) for 24 h to remove both the silica rods and glass substrate.

Characterization: The microstructures are imaged using Hitachi S4800 and JEOL 7000s SEMs. FIB characterization is performed in a FEI Dual Beam 235.

Supporting Information

Supporting Information is available from the Wiley Online Library or from the author.

Acknowledgments

Colloidal rod synthesis was primarily supported by the U.S. Department of Energy, Division of Materials Sciences under Award No. DE-FG02–07ER46471, through the Frederick Seitz Materials Research Laboratory at the University of Illinois at Urbana-Champaign. Vertical and horizontal rod template assembly and templating was primarily supported by an AFOSR MURI (FA9550–12–1–0471).

Received: September 25, 2013
Revised: October 27, 2013
Published online: December 23, 2013

[1] A. P. Hynninen, J. H. J. Thijssen, E. C. M. Vermolen, M. Dijkstra, A. Van Blaaderen, *Nat. Mater.* **2007**, *6*, 202.
[2] E. C. Nelson, N. L. Dias, K. P. Bassett, S. N. Dunham, V. Verma, M. Miyake, P. Wiltzius, J. A. Rogers, J. J. Coleman, X. L. Li, P. V. Braun, *Nat. Mater.* **2011**, *10*, 676.
[3] a) H. G. Zhang, P. V. Braun, *Nano Lett.* **2012**, *12*, 2778; b) H. G. Zhang, X. D. Yu, P. V. Braun, *Nature Nanotech.* **2011**, *6*, 277; c) N. Tetreault, E. Arsenault, L. P. Heiniger, N. Soheilnia, J. Brillet, T. Moehl, S. Zakeeruddin, G. A. Ozin, M. Grätzel, *Nano Lett.* **2011**, *11*, 4579.
[4] a) H. Nguyen, S. A. El-Safty, *J. Phys. Chem. C* **2011**, *115*, 8466; b) J. Y. Wang, Y. Cao, Y. Feng, F. Yin, J. P. Gao, *Adv. Mater.* **2007**, *19*, 3865.
[5] a) M.-Y. Tsang, N. E. Pridmore, L. J. Gillie, Y.-H. Chou, R. Brydson, R. E. Douthwaite, *Adv. Mater.* **2012**, *24*, 3406; b) J. Liang, Y. Zheng, J. Chen, J. Liu, D. Hulicova-Jurcakova, M. Jaroniec, S. Z. Qiao, *Angew. Chem.-Int. Ed.* **2012**, *51*, 3892.
[6] a) D. Xia, Z. Ku, S. C. Lee, S. R. J. Brueck, *Adv. Mater.* **2011**, *23*, 147; b) Y. C. Chen, J. B. Geddes, L. L. Yin, P. Wiltzius, P. V. Braun, *Adv. Mater.* **2012**, *24*, 2863.
[7] D. Chanda, K. Shigeta, S. Gupta, T. Cain, A. Carlson, A. Mihi, A. J. Baca, G. R. Bogart, P. Braun, J. A. Rogers, *Nat. Nanotech.* **2011**, *6*, 402.
[8] L. Chuenchom, R. Kraehnert, B. M. Smarsly, *Soft Matter* **2012**, *8*, 10801.
[9] a) A. Radke, T. Gissibl, T. Klotzbucher, P. V. Braun, H. Giessen, *Adv. Mater.* **2011**, *23*, 3018; b) J. A. Lewis, *Adv. Funct. Mater.* **2006**, *16*, 2193; c) J. A. Lewis, J. E. Smay, J. Stuecker, J. Cesarano, *J. Am. Ceram. Soc.* **2006**, *89*, 3599; d) M. Deubel, G. Von Freymann, M. Wegener, S. Pereira, K. Busch, C. M. Soukoulis, *Nat. Mater.* **2004**, *3*, 444.
[10] D. C. Meisel, M. Diem, M. Deubel, F. Perez-Willard, S. Linden, D. Gerthsen, K. Busch, M. Wegener, *Adv. Mater.* **2006**, *18*, 2964.
[11] a) W. H. Peng, S. M. Zhu, W. L. Wang, W. Zhang, J. J. Gu, X. B. Hu, D. Zhang, Z. X. Chen, *Adv. Funct. Mater.* **2012**, *22*, 2072; b) Y. W. Tan, J. J. Gu, X. N. Zang, W. Xu, K. C. Shi, L. H. Xu, D. Zhang, *Angew. Chem.-Int. Ed.* **2011**, *50*, 8307; c) D. Van Opdenbosch, M. Johannes, X. Wu, H. Fabritius, C. Zollfrank, *Photonics and Nanostructures-Fundamentals and Applications* **2012**, *10*, 516; d) J. W. Galusho, M. R. Jorgensen, M. H. Bartl, *Adv. Mater.* **2010**, *22*, 107.
[12] a) B. Z. Tian, J. Liu, T. Dvir, L. H. Jin, J. H. Tsui, Q. Qing, Z. G. Suo, R. Langer, D. S. Kohane, C. M. Lieber, *Nat. Mater.* **2012**, *11*, 986; b) J. P. Hoogenboom, C. Retif, E. de Bres, M. V. de Boer, A. K. van Langen-Suurling, J. Romijn, A. van Blaaderen, *Nano Lett.* **2004**, *4*, 205.
[13] A. Stein, F. Li, N. R. Denny, *Chemistry of Materials* **2008**, *20*, 649.
[14] a) J. G. Park, M. Mittal, H. Noh, C. F. Schreck, C. S. O'Hern, H. Cao, E. M. Furst, E. R. Dufresne, *ACS Nano* **2011**, *5*, 6695; b) T. Ding, K. Song, K. Clays, C. H. Tung, *Adv. Mater.* **2009**, *21*, 1936.
[15] a) S. M. Reddy, J. J. Park, S. M. Na, M. M. Maqableh, A. B. Flatau, B. J. H. Stadler, *Adv. Funct. Mater.* **2011**, *21*, 4677; b) X. S. Gao, B. J. Rodriguez, L. F. Liu, B. Birajdar, D. Pantel, M. Ziese, M. Alexe, D. Hesse, *ACS Nano* **2010**, *4*, 1099.
[16] X. Chen, M. Steinhart, C. Hess, U. Gosele, *Adv. Mater.* **2006**, *18*, 2153.
[17] a) K. Chaudhary, Q. Chen, J. J. Juarez, S. Granick, J. A. Lewis, *J. Am. Chem. Soc.* **2012**, *134*, 12901; b) J. Yan, K. Chaudhary, S. C. Bae, J. A. Lewis, S. Granick, *Nat. Commun.* **2013**, *4*; c) J. H. Zhang, H. Y. Liu, Z. L. Wang, N. B. Ming, *Chem. Eur. J.* **2008**, *14*, 4374.
[18] A. Kuijk, A. van Blaaderen, A. Imhof, *J. Am. Chem. Soc.* **2011**, *133*, 2346.
[19] W. Stöber, A. Fink, E. Bohn, *J. Coll. Interf. Sci.* **1968**, *26*, 62.
[20] a) M. J. Solomon, *Current Opinion in Colloid & Interface Science* **2011**, *16*, 158; b) K. Kang, J. K. G. Dhont, *Soft Matter* **2010**, *6*, 273; c) M. L. Pedano, S. Z. Li, G. C. Schatz, C. A. Mirkin, *Angew. Chem.-Int. Ed.* **2010**, *49*, 78; d) A. A. Shah, H. Kang, K. L. Kohlstedt, K. H. Ahn, S. C. Glotzer, C. W. Monroe, M. J. Solomon, *Small* **2012**, *8*, 1551; e) Z. Y. Zou, X. J. Chen, Q. Wang, S. L. Qu, X. Y. Wang, *J. Appl. Phys.* **2008**, *104*; f) F. D. Ma, S. J. Wang, L. Smith, N. Wu, *Adv. Funct. Mater.* **2012**, *22*, 4334; g) M. I. Bodnarchuk, M. V. Kovalenko, W. Heiss, D. V. Talapin, *J. Am. Chem. Soc.* **2010**, *132*, 11967.
[21] T. B. Jones, *Electromechanics of Particles*, Cambridge University Press, Cambridge, U.K.
[22] Y. Solomentsev, S. A. Guelcher, M. Bevan, J. L. Anderson, *Langmuir* **2000**, *16*, 9608.
[23] G. E. Fernandes, D. J. Beltran-Villegas, M. A. Bevan, *Langmuir* **2008**, *24*, 10776.
[24] A. Brzezinski, Y. C. Chen, P. Wiltzius, P. V. Braun, *J. Mater. Chem.* **2009**, *19*, 9126.
[25] J. J. Juarez, S. E. Feicht, M. A. Bevan, *Soft Matter* **2012**, *8*, 94.
[26] D. R. Nelson, B. I. Halperin, *Phys. Rev. B* **1979**, *19*, 2457.
[27] S. van Teeffelen, C. N. Likos, H. Lowen, *Phys. Rev.Lett.* **2008**, *100*.